Journal of Magnetic Resonance **143,** 17–23 (2000)
doi:10.1006/jmre.1999.1984, available online at http://www.idealibrary.com on IDEAL®

Three-Dimensional ^{13}C-Spectroscopic Imaging in the Isolated Infarcted Rat Heart

Claudia Weidensteiner, Titus Lanz, Michael Horn,* Stefan Neubauer,* Axel Haase, and Markus von Kienlin

*Department of Physics and *Department of Medicine, University of Würzburg, 97074 Würzburg, Germany*

Received October 16, 1998; revised July 9, 1999

Acquisition weighted ^{13}C-spectroscopic imaging with three spatial dimensions is demonstrated in the isolated, perfused rat heart. Experiments were performed at 11.75 T with a homebuilt double resonant ^{13}C–^{1}H probehead. Three-dimensional chemical shift imaging was used to obtain ^{1}H-decoupled ^{13}C-spectra in 96-μl voxels in about 58 min. Acquisition weighting significantly reduced signal contamination and improved image quality, with no penalty in sensitivity. As a first application, infarcted hearts were studied during perfusion with [2-^{13}C]-sodium acetate. The extent of the incorporation of the ^{13}C-label into glutamate allows us to distinguish intact and infarcted myocardium. Chemical shift images show a homogeneous glutamate distribution in intact tissue, but a neglible amount in the infarction scar.

Key Words: **isolated rat heart; carbon-13; chemical shift imaging; acquisition weighting; myocardial infarction.**

1. INTRODUCTION

^{13}C NMR spectroscopy is a powerful method for investigating cardiac metabolism *in vivo.* ^{13}C has a low natural abundance. Therefore it is possible to examine specific metabolic pathways with tracers, that is, with ^{13}C-enriched compounds. Most of these studies are performed in animal models, where, for instance, the time course of ^{13}C-enrichment in the pathways can be followed with ^{13}C MRS, which allows one to determine metabolic flux rates (*1–5*). The ^{13}C-labeling in the end-products can also be detected to study substrate selection in the heart (*2, 6*).

Spatially resolved ^{13}C spectroscopy in the heart makes it possible to investigate the effect of regional cardiac injury such as acute regional ischemia or infarction on substrate metabolism. This is difficult, however, due to the poor NMR sensitivity of ^{13}C. So far spatially resolved ^{13}C spectroscopy in the heart has only been reported with one spatial dimension (*7, 8*).

Three-dimensional chemical shift imaging (3D CSI), (*9, 10*) provides a method of resolving metabolic information in form of images and of spectra in all voxels. The localization in 3D CSI with phase encoding gradients in three dimensions is preferable to methods using selective excitation because of the large chemical shifts of ^{13}C, which would cause severe artifacts.

The extent of signal contamination between adjacent voxels—and therefore image quality and localization—in CSI depends on the spatial response function (SRF). The SRF shows how every location in the object contributes to the signal in a specific voxel of the chemical shift image.

With acquisition weighted CSI (*11, 12*) the shape of the SRF can be improved in comparison to conventional CSI. Therefore signal contamination can be significantly reduced, which is particularly important in situations like the measurement of regional ^{13}C-metabolite content in the isolated rat heart, where the spatial resolution is close to the size of the anatomical structures.

Using acquisition weighted CSI we performed the first 3D ^{13}C CSI reported in the isolated normal and infarcted rat heart. We achieved the necessary sensitivity for this experiment with a homebuilt, double-tuned probehead (*13, 14*) on a 11.75-T NMR microscopy system.

2. METHODS

2.1. Heart Perfusion

The experiments were performed in normal and in chronically infarcted hearts of male Wistar rats. All studies were performed under the guidelines of the American Physiological Society. The rats that were designated for infarction were anesthetized and subjected to ligation of the left anterior descending artery as previously described (*15, 16*). After 4 weeks the hearts were excised for NMR examination.

All hearts were perfused in the Langendorff mode with a constant pressure of 100 mm Hg. The perfusate was equilibrated with 95% O_2/5% CO_2, yielding a pH of 7.4, and maintained at 37°C. During experimental setup the hearts were perfused with Krebs–Henseleit buffer containing 11 mM unenriched glucose. Afterward, the perfusate was switched to Krebs–Henseleit buffer containing 5 mM 99% enriched [2-^{13}C]-sodium acetate. One liter of this solution was recirculated for about 90 min. The CSI experiment was started 15 min after onset of the ^{13}C-perfusion in order to ensure steady-state conditions.

The hearts contracted spontaneously against a water-filled vinyl balloon in the left ventricle. The balloon was connected to a Statham P23 Db pressure transducer. Heart rate, left

1090-7807/00 $35.00

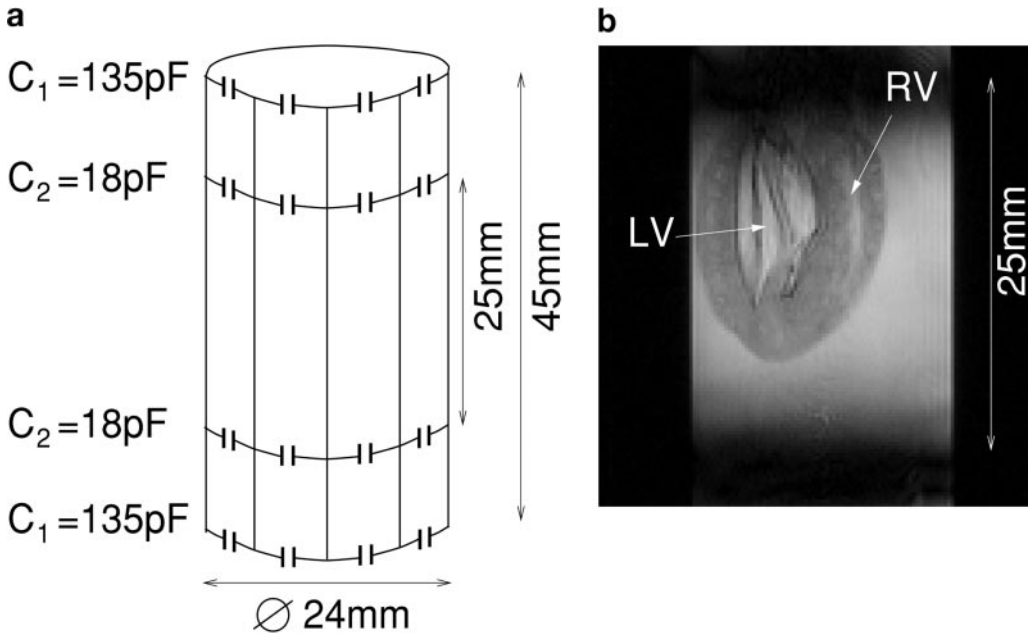

FIG. 1. (a) Schematic drawing of the double-tuned four-ring birdcage resonator, specifying its dimensions and the values of the capacitors. This resonator is sensitive for both ^{13}C and ^{1}H between the two inner rings. (b) Longitudinal ^{1}H-FLASH image (256 × 256 pixels, FOV 6 × 6 mm) of an isolated rat heart acquired with this resonator. The right ventricle (RV) is collapsed; the left ventricle (LV) is filled by a water-filled vinyl balloon.

ventricular developed pressure, and coronary flow were continuously monitored. A trigger signal derived from the pressure curve served to synchronize the MR spectrometer to the heart cycle.

2.2. Histology of Infarcted Hearts

The infarct size was determined histologically as previously described (*17*). After MR imaging, the infarcted hearts were embedded in paraffin and cut in 20-μm sections (slice separation 1 mm). The sections were stained with Picrosirius Red. Scarred tissue stains red, whereas viable myocardium does not. The stained sections were mounted on slides and digitally scanned.

2.3. Probehead

All experiments were performed on a Bruker AMX-500 microscopy system using a double-tuned homebuilt probehead with the ^{13}C–^{1}H four-ring birdcage resonator shown in Fig. 1 (*14, 18*). We chose a highpass–highpass birdcage design to minimize dielectric losses in the sample. This eight-rung four-ring birdcage is made of 80-μm copper foil and 135 pF/18 pF chip capacitors (ATC) mounted on a glass tube with 24-mm outer diameter. The inner rings of the birdcage are 25 mm apart; its overall length is 45 mm. The ^{13}C- and ^{1}H-sensitive volume of the resonator covers the whole heart. A capacitive coupling scheme combined with triaxial baluns ensures full electrical balance of the circuit. The isolation between the ^{13}C-quadrature channels is −24 dB. Quadrature drive increases the sensitivity theoretically by a factor of $\sqrt{2}$ (*19*). The *Q*-values of the unloaded resonator are 170 and 195 for the quadrature ^{13}C-channels and 164 for the linearly driven ^{1}H-channel. These values drop to 123/139 and 82, respectively, when the birdcage is loaded with a 19-mm tube containing physiological saline solution. The ^{1}H-channel of the resonator is used for shimming, FLASH-imaging of the heart, and the double-resonance techniques.

2.4. ^{1}H-Imaging

For anatomical information ^{1}H-images were acquired with a modified FLASH sequence (*17, 20*). The matrix size was 256 × 256 with a slice thickness of 1 mm. The FOV of the transversal images was 32 mm × 32 mm (identical to the FOV of the ^{13}C-images) and 60 mm × 60 mm for the longitudinal images. Four averages were acquired with a repetition time of 125 ms. An off-resonant magnetization transfer contrast pulse (*17, 21*) prior to excitation enhances the contrast between tissue and perfusate. The sequence was synchronized to the heart cycle.

2.5. 3D ^{13}C CSI

The pulse sequence of the 3D CSI experiment is shown in Fig. 2. The protocol was synchronized to the heart cycle. Ten 180° pulses (interpulse delay 0.1 s) prior to the ^{13}C-excitation were applied to saturate the ^{1}H-spins for nuclear Overhauser enhancement. The pulse angle for the ^{13}C-excitation was 77°. With T_1 = 1.16 s for the glutamate–C4 resonance in the rat heart (*22*) this is the Ernst angle for the given repetition time of 1.5 s. Repetition time varied slightly because of the synchro-

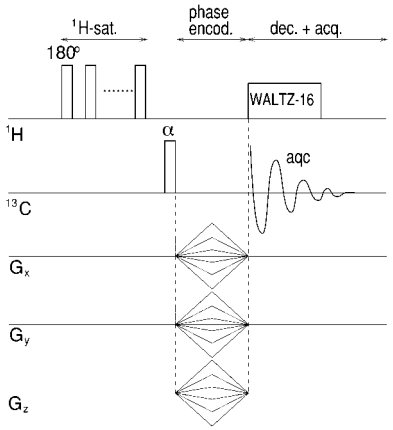

FIG. 2. The ^{13}C CSI sequence with ^{1}H-saturation prepulses for NOE and WALTZ-16 decoupling. Spatial localization is achieved with triangular pulsed gradients in all spatial directions.

nization to the heart cycle. The experimental time for both the conventional and the acquisition weighted CSI protocol varied between 55 and 60 min. The phase encoding was performed in 310 μs immediately after the ^{13}C-excitation. A total of 1024 complex data points were acquired in the spectroscopic dimension over a bandwidth of 8.6 kHz. During phase encoding the first 3 complex data points of the FID are lost. ^{1}H-decoupling of the ^{13}C-resonances was achieved with a WALTZ-16 sequence (*23*) during the first 60 ms of the acquisition time. The ^{1}H-prepulses and the decoupling cause an Overhauser enhancement of about 2.4.

The average RF power applied during the ^{13}C CSI experiment was 0.4 W. With a sample volume of approximately 12 ml (heart + surrounding perfusate) and the *Q*-values of the birdcage the specific absorption rate in the ^{13}C CSI experiment was calculated according to (*24*) to be approximately 17 W/kg. Although this is higher than the FDA guideline of 8 W/kg spatial peak (*25*), overheating of the heart was avoided since the circulating perfusate keeps the heart at 37°C. Furthermore, the heart rate did not change during the CSI experiment, which would indicate a temperature rise in the tissue.

In conventional 3D CSI the number of averages at each value of the phase encoding gradients—the gradient weighting function—is constant. The nominal spatial resolution is defined by the spatial response function, which is the Fourier transform of this gradient weighting function. It is well known that the SRF in a conventional CSI experiment is a sinc-like function with considerable sidebands (see Fig. 3a).

Using a Hanning window as the weighting function of *k*-space (*11, 12*) modifies the shape of the SRF and reduces its sidebands (see Fig. 3c). In the same way the point spread function (PSF) is modified. The PSF has the same shape as the SRF and shows how the signal coming from a specific point source in the object is spread over the chemical shift image. A chemical shift image is the result of the convolution of the spin distribution map with the PSF. A PSF with considerable sidebands leads to an interference pattern in the chemical shift image, especially when the size of the geometric structures is similar to the nominal resolution. The effect of an improved SRF/PSF on image quality can be seen in Fig. 4. The spin distribution (a) is assumed to be uniform within the contours taken from the heart in Fig. 5 (top). The convolution was calculated with the PSFs shown in Fig. 3. The interference pattern of the simulated conventional image can be easily seen in Fig. 4b, both within the heart contours and in the background. The simulated acquisition weighted image shown in Fig. 4c is more homogeneous, better reflecting the uniform spin distribution.

In acquisition weighted CSI (*11, 12*) the weighting is already performed during acquisition: the number of averages of the different phase encoding gradients corresponds to the value of the Hanning window at this point in *k*-space. The acquisition weighting avoids the penalty in sensitivity from which post-processing filtering techniques suffer.

We acquired the conventional 3D ^{13}C CSI datasets with 8 × 8 × 8 phase encoding steps (four averages, total number of

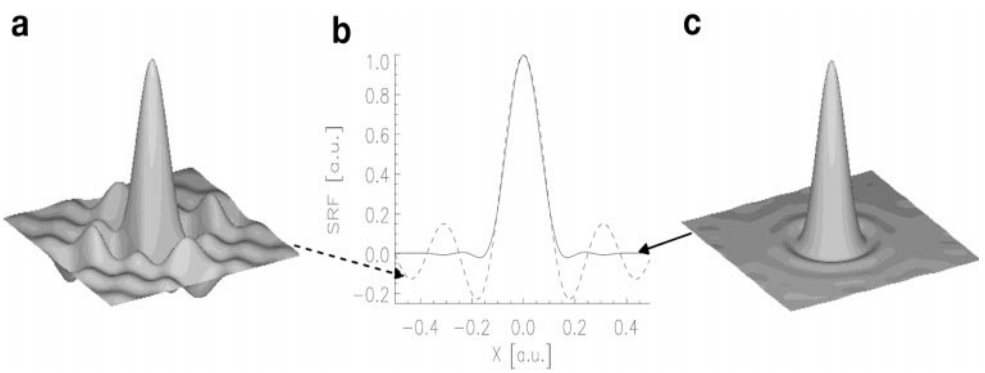

FIG. 3. Calculated SRF of the conventional (a) and acquisition weighted (c) CSI experiment in the central, transversal slice of the 3D dataset. Acquisition weighting decreases the relative height of the side bands of the SRF considerably. Overlaying the profile of the two SRFs (conventional: dashed) in (b) shows their identical width, which means that both experiments have the same nominal spatial resolution. The PSF of the experiment has exactly the same shape as the SRF.

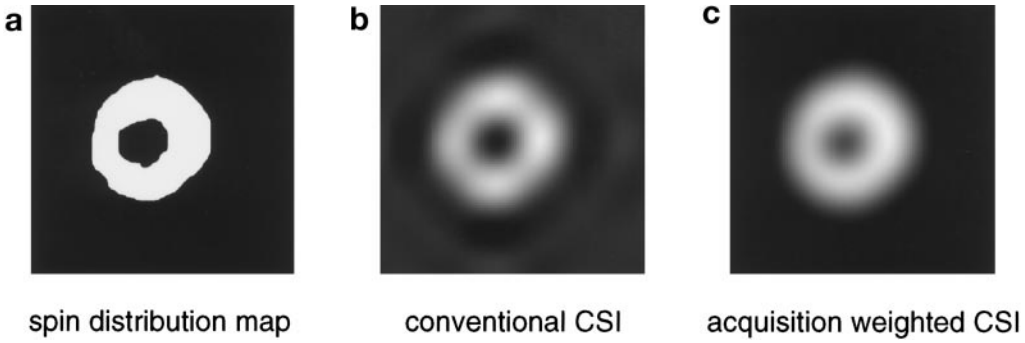

FIG. 4. Simulated conventional (b) and acquisition weighted (c) chemical shift images of an uniform spin distribution map (a) (heart contours taken from Fig. 5, top). The images were calculated by convoluting the spin distribution map with the PSFs of the conventional and the acquisition weighted CSI experiment (having the same shape as the SRFs in Fig. 3). The simulated conventional image shows a striking interference pattern both within the heart contours and in the background, which compares well to the measured ^{13}C-map in Fig. 5 (top). The simulated acquisition weighted chemical shift image (c) displays a much more homogeneous distribution within the heart contours and no background signal.

scans 2048). The FOV in the x-/y-/z-direction was 32 × 32 × 48 mm. This results in a nominal spatial resolution of 4 mm in the x- and y-direction and 6 mm in the z-direction (voxel size 96 μl). The calculated SRF of this experiment is shown in Fig. 3a. The experiments were performed in three intact hearts.

For the acquisition weighted 3D ^{13}C CSI datasets a total number of 1976 scans was acquired. The Hanning function was adjusted to yield an identical width of the central part of the SRF that means to achieve the same nominal spatial resolution as in the conventional experiment (4 mm in the x- and y-

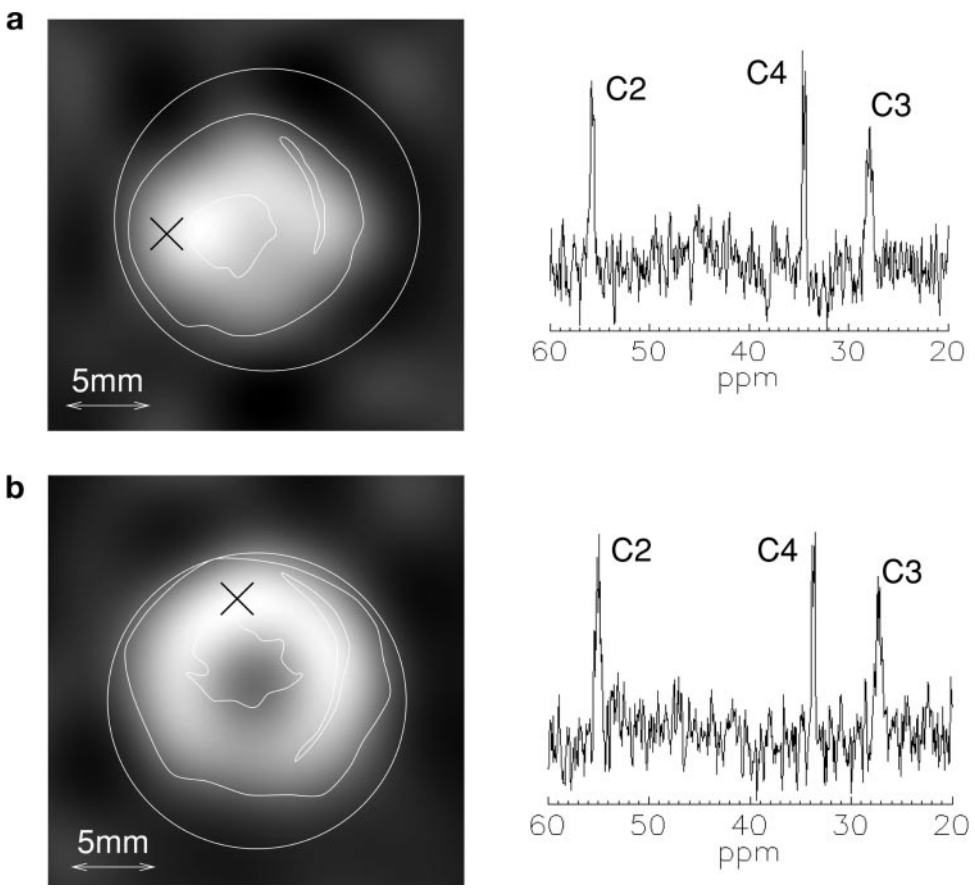

FIG. 5. Comparison between conventional (a) and acquisition weighted (b) ^{13}C-chemical shift images of the glutamate–C4 distribution in transversal slices of two normal, isolated rat hearts. These images clearly demonstrate the reduced signal contamination in acquisition weighted CSI. The contours of the NMR tube, the heart, the collapsed right ventricle, and the pressure balloon in the left ventricle are taken from the corresponding ^{1}H-images. The ^{1}H-decoupled ^{13}C-spectra show the glutamate resonances in the indicated voxels. The SNR of both spectra is identical, as is the nominal voxel size of 96 μl.

direction and 6 mm in the *z*-direction), as can be seen in Fig. 3. Thus, 437 different phase encoding steps were performed for a FOV of 32 × 32 × 48 mm. The maximum number of phase encoding steps in a spatial dimension was 13. The number of averages in the middle of the *k*-space was 8. The acquisition weighted experiments were performed in three intact and in one infarcted heart.

2.6. Processing

Weighting during acquisition involves an integer number of averages. To reduce this digitization error, the acquisition weighted CSI datasets were postweighted according to the real Hanning window. The conventional and the acquisition weighted CSI datasets were zero filled to a matrix size of 256 × 256 × 64 and filtered with an exponential function (LB = 10 Hz) in the spectroscopic dimension. After a 4-dimensional Fourier transformation a manual zero- and first-order phase correction in the spectroscopic dimension and a theoretically determined phase correction in the spatial dimensions were performed. The ^{13}C-maps were obtained after integration of the central peak area of the resonance of interest and displaying the integrals as a grayscale image.

For anatomical reference, the contours of the heart, balloon, and ventricles were traced on the ^{1}H-image of the corresponding slice and superimposed onto the ^{13}C-maps.

3. RESULTS

The ^{13}C-label of acetate is incorporated into glutamate via the tricarboxylic acid cycle. Global spectra show that 15 min after onset of ^{13}C-perfusion the peak area and the multiplet structure of the glutamate–C4 resonance have reached steady state (*26*).

The spectroscopic images in Fig. 5 show the distribution of the glutamate–C4 resonance in transversal slices of a control heart. The upper image was acquired with conventional CSI, the lower one with acquisition weighted CSI in another heart.

The conventional image shows the interference pattern similar to the one in the simulated chemical shift image in Fig. 4b. The distribution of the glutamate signal in the acquisition weighted spectroscopic image does not show this pattern and corresponds better to the shape of the myocardium. Therefore, the positive effect of acquisition weighting due to the improved SRF is demonstrated in these experiments.

The two ^{1}H-decoupled ^{13}C-spectra of the conventional (a) and of the acquisition weighted (b) dataset correspond to the indicated voxels in the myocardium. The signal-to-noise ratio of both spectra is the same. Acquisition weighting does not reduce the sensitivity whereas it reduces the signal contamination. Since the total number of scans is approximately the same in both experiments, this result is expected from theory.

Figure 6 shows spectroscopic images of the glutamate–C4 resonance in two different transversal slices extracted from the 3D dataset acquired in a chronically infarcted heart. The infarcted area can be identified in the corresponding ^{1}H-images due to the reduced wall thickness of the myocardium. The histology shows that the infarcted, scarred areas stained by Picrosirius Red have different sizes: they are bigger in (a), which is closer to the apex, than in (b). The size of the signal void in the ^{13}C-maps corresponds to the infarct size determined by histology: the signal void is bigger in slice (a) than in slice (b). In the residual intact myocardium the glutamate distribution is uniform within the obtained SNR. In contrast to spectrum (c) from intact tissue, spectrum (d) from scarred tissue shows the absence of glutamate peaks in the infarcted region. Therefore, in the model of the infarcted rat heart, intact and infarcted myocardium can be distinguished due to the extend of incorporation of the ^{13}C-label into glutamate.

4. DISCUSSION

The purpose of the present work was to demonstrate high-resolution 3D spectroscopic imaging of ^{13}C-enriched metabolites in isolated rat hearts at high magnetic field. With the optimization of the homebuilt probehead and the combination of CSI with double-resonance techniques, we obtained the necessary sensitivity to perform the first 3D ^{13}C CSI experiment in isolated intact and infarcted rat hearts ever.

The signal-to-noise ratio of our setup should be sufficient to measure the regional ^{13}C-metabolite content. The visibility of the multiplet structure of the glutamate peaks makes an isotopomer analysis of the tricarboxylic acid cycle possible.

Acquisition weighting can dramatically reduce signal contamination without a loss in sensitivity. Compared to conventional CSI, a higher image quality and identical SNR were achieved in the same experimental time. The reduction of contamination—which means improved localization—is an essential prerequisite for a correct, spatially resolved measurement of metabolites.

To demonstrate the potential of acquisition weighted ^{13}C CSI to detect regional cardiac injury we performed this technique in chronically infarcted rat hearts. Scarred and intact tissue can be clearly distinguished. The results of ^{13}C CSI correspond to the results of the Picrosirius Red staining. The experiments demonstrate that acetate is not metabolized in myocardial scar tissue. It appears that this method can serve as a tool for measuring infarct size.

So far, we have used ^{13}C-labeled acetate as substrate which allows us to examine the oxidative metabolism. Regions deprived of oxygenated perfusate, i.e., ischemic, infarcted and scarred regions, cannot metabolize acetate to glutamate. Therefore, these injuries can be detected with our method. However, necrotic and ischemic (nonviable and viable) tissue cannot be distinguished by the use of acetate.

3D ^{13}C CSI can be used for investigation of regional changes in ^{13}C-metabolism in the isolated rat heart, a standard model of cardiac research. At present, the long experimental duration (55 to 60 min) of this kind of experiment only allows one to examine steady state. The high sensitivity of our probehead can

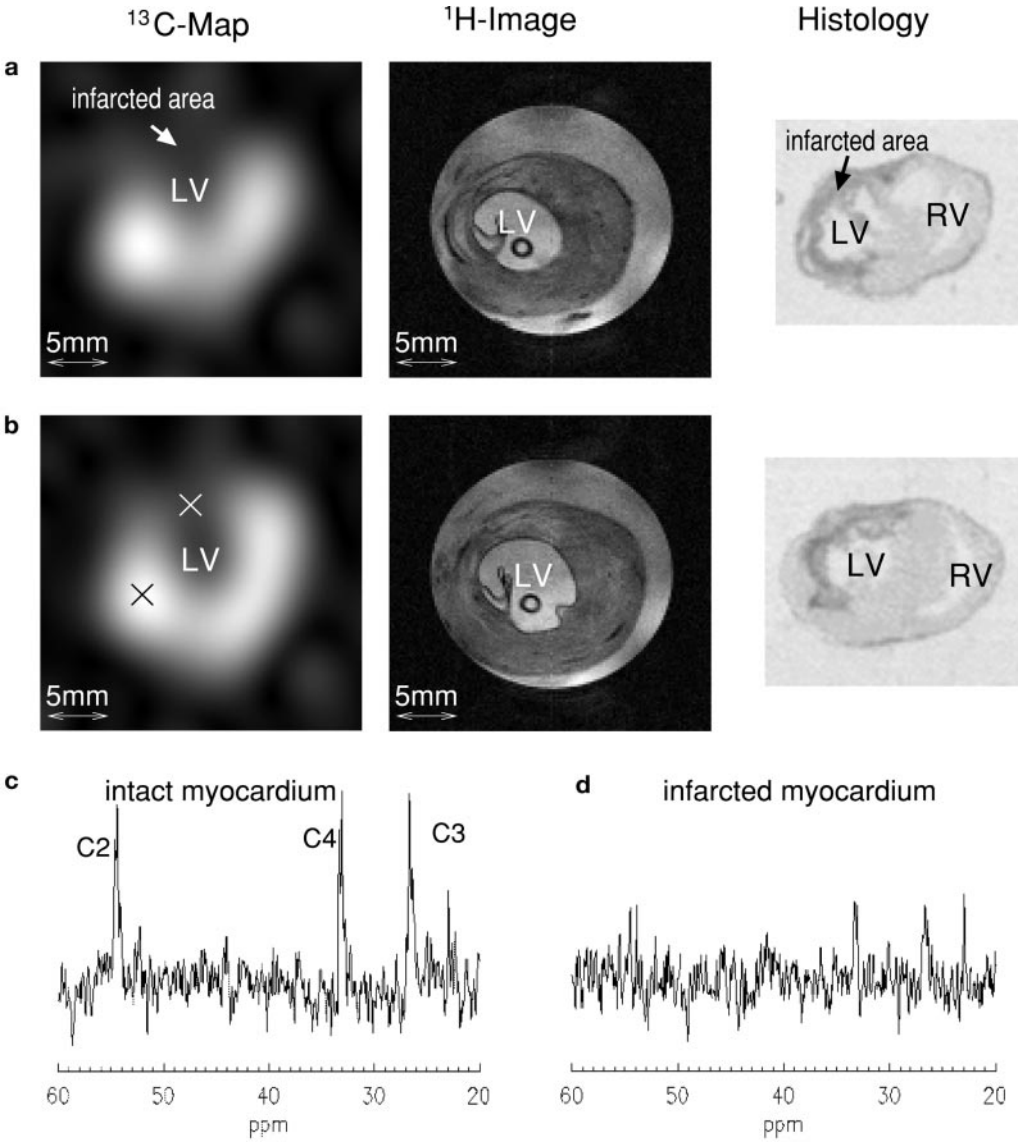

FIG. 6. Acquisition weighted ^{13}C-chemical shift images of the glutamate–C4 resonance in two transversal slices (slice separation 2 mm, slice (a) closer to the apex) of an isolated, chronically infarcted rat heart. The ^{1}H-images and the histological sections (infarcted areas stained with Picrosirius Red) correspond to the ^{13}C-image slices. The infarcted area in the ^{13}C-images can be identified due to the absence of the glutamate signal. The ^{1}H-decoupled ^{13}C-spectra (c) and (d) are obtained from voxels marked by a cross in intact (showing the glutamate resonances C2, C3, and C4) and scarred tissue in slice (b).

also be used for unlocalized, kinetic analysis of metabolic turnover with a high temporal resolution.

ACKNOWLEDGMENTS

The authors thank Elsbeth Fekete for her help with the heart preparation, Charlotte Dienesch and Andrea Leupold for performing the coronary artery ligation, and Michaela Hartmann for the histology. Many thanks to Yann Le Fur for the software to process the acquisition weighted datasets. Thanks to Craig Malloy for stimulating discussions. This work was supported by Deutsche Forschungsgemeinschaft (C.W., T.L.: GRK 64; M.v.K.: Ki 433/2-2, Ki 433/2-3) and Bundesministerium für Bildung, Wissenschaft, Forschung und Technologie (M.H., S.N.: Interdisziplinäres Zentrum für klinische Forschung 01KS9603).

REFERENCES

1. C. R. Malloy, A. D. Sherry, and F. M. Jeffrey, Carbon flux through citric acid cycle pathways in perfused heart by ^{13}C NMR spectroscopy, *FEBS Lett.* **212,** 58–62 (1987).
2. C. R. Malloy, A. D. Sherry, and F. M. Jeffrey, Evaluation of carbon flux and substrate selection through alternate pathways involving the citric acid cycle of the heart by ^{13}C NMR spectroscopy, *J. Biol. Chem.* **263,** 6964–6971 (1988).
3. R. G. Weiss, S. T. Gloth, R. Kalil-Filho, V. P. Chacko, M. D. Stern, and G. Gerstenblith, Indexing tricarboxylic acid cycle flux in intact hearts by carbon-13 nuclear magnetic resonance, *Circ. Res.* **70,** 392–408 (1992).
4. X. Yu, L. T. White, C. Doumen, L. A. Damico, K. F. LaNoue, N. M. Alpert, E. D. Lewandowski, Kinetic analysis of dynamic ^{13}C NMR

spectra: Metabolic flux, regulation, and compartimentation in hearts, *Biophys. J.* **69,** 2090–2102 (1995).

5. X. Yu, L. T. White, N. M. Alpert, E. D. Lewandowski, Subcellular metabolite transport and carbon isotope kinetics in the intramyocardial glutamate pool, *Biochemistry* **35,** 6963–6968 (1996).
6. A. D. Sherry, P. Zhao, A. Wiethoff, C. R. Malloy, ^{13}C isotopomer analyses in intact tissue using {^{13}C} homonuclear decoupling, *Magn. Reson. Med.* **31,** 374–379 (1994).
7. P. A. Bottomley, C. J. Hardy, P. B. Roemer, O. M. Mueller, Proton-decoupled, Overhauser-enhanced, spatially localized carbon-13 spectroscopy in humans, *Magn. Reson. Med.* **12,** 348–363 (1989).
8. A. M. Abduljalil, D. P. Rath, Z. Hui, A. H. Aletras, W. C. McCartney, P. M. Robitaille, Spatial localization with modified Fourier series windows. Application to the transmural ^{13}C-nuclear magnetic resonance analysis of the in vivo myocardium, *Invest. Radiol.* **31**(10), 611–618 (1996).
9. T. R. Brown, B. M. Kincaid, K. Ugurbil, NMR chemical shift imaging in three dimensions, *Proc. Natl. Acad. Sci. USA* **79,** 3523–3526 (1982).
10. A. A. Maudsley, S. K. Hilal, W. H. Perman, H. E. Simon, Spatially resolved high-resolution spectroscopy by "four-dimensional" NMR, *J. Magn. Reson.* **51,** 147–152 (1983).
11. T. H. Mareci, H. R. Brooker, High-resolution magnetic resonance spectra from a sensitive region defined with pulsed field gradients, *J. Magn. Reson.* **57**(1), 157–246 (1984).
12. T. H. Mareci, H. R. Brooker, Essential considerations for spectral localization using indirect gradient encoding of spatial information, *J. Magn. Reson.* **92,** 229–246 (1991).
13. T. Lanz, M. v. Kienlin, C. Weidensteiner, A. Haase, A double tuned, circular polarized ^{13}C–^{1}H-four-ring birdcage resonator, *in* "Proc., ESMRMB, 14th Annual Meeting, Bruxelles 1997," p. 93.
14. T. Lanz, M. v. Kienlin, W. Behr, A. Haase, A double tuned, circular polarized ^{31}P–^{1}H-four-ring birdcage resonator, *MAGMA* **5,** 243–246 (1997).
15. M. A. Pfeffer, J. M. Pfeffer, M. C. Fischbein, P. J. Fletcher, J. Spadaro, R. A. Kloner, E. Braunwald, Myocardial infarct size and ventricular function in rats, *Circ. Res.* **44,** 503–512 (1979).
16. P. Gaudron, M. Blumrich, G. Ertl, Aggravation of left ventricular dilatation and reduction of survival by a calcium channel blocker in rats with chronic myocardial infarction, *Am. Heart J.* **125,** 1226–1233 (1993).
17. M. von Kienlin, C. Rösch, Y. Le Fur, W. Behr, F. Roder, A. Haase, M. Horn, B. Illing, K. Hu, G. Ertl, and S. Neubauer, Three-dimensional ^{31}P magnetic resonance spectroscopic imaging of regional high-energy phosphate metabolism in injured rat heart, *Magn. Reson. Med.* **39,** 731–741 (1998).
18. J. Murphy-Boesch, R. Srinivasan, L. Carvajal, T. R. Brown, Two configurations of the four-ring birdcage coil for ^{1}H-imaging and ^{1}H-decoupling, *J. Magn. Reson. B* **103,** 103–114 (1994).
19. C.-N. Chen, D. I. Hoult, V. J. Sank, Quadrature detection coils—A further $\sqrt{2}$ improvement in sensitivity, *J. Magn. Reson.* **54,** 324–327 (1983).
20. A. Haase, J. Frahm, D. Matthei, W. Hanicke, K. D. Merboldt, FLASH-imaging: Rapid NMR imaging using low flip angle pulses, *J. Magn. Reson.* **67,** 258–266 (1986).
21. S. D. Wolff, R. S. Balaban, Magnetization transfer contrast (MTC) and tissue water proton relaxation *in vivo, Magn. Reson. Med.* **10,** 135–144 (1989).
22. A. D. Sherry, B. Sumegi, B. Miller, G. L. Cottam, S. Gavva, J. G. Jones, C. R. Malloy, Orientation-conserved transfer of symmetric Krebs cycle intermediates in mammalian tissue, *Biochemistry* **33,** 6268–6275 (1994).
23. A. J. Shaka, J. Keeler, R. Freeman, Evaluation of a new broad-band decoupling sequence: WALTZ-16, *J. Magn. Reson.* **53,** 313–340 (1983).
24. P. A. Bottomley, R. W. Redington, W. A. Edelstein, J. F. Schenk, Estimating radiofrequency power deposition in body NMR imaging, *Magn. Reson. Med.* **2,** 336–349 (1985).
25. Food and Drug Administration, Magnetic resonance diagnostic device, Panel recommendation and report on petitions for MR reclassification, *Fed. Reg.* **53,** 7575–7579 (1988).
26. C. Weidensteiner, T. Lanz, A. Haase, M. v. Kienlin, ^{13}C-Spectroscopic imaging in the isolated rat heart at 11.75 T, *in* "Proc., ISMRM, 6th Annual Meeting, Sydney, 1998," p. 359.